

Femtosecond IR Spectroscopy of Peroxycarbonate Photodecomposition: S₁-Lifetime Determines Decarboxylation Rate

Christian Reichardt,[†] Jörg Schroeder,^{†,‡} and Dirk Schwarzer^{*,†}

Abteilung Spektroskopie und Photochemische Kinetik, Max-Planck-Institut für Biophysikalische Chemie, 37070 Göttingen, Germany, and Institut für Physikalische Chemie, Universität Göttingen, Tammannstrasse 6, 37077 Göttingen, Germany

Received: June 4, 2007; In Final Form: July 25, 2007

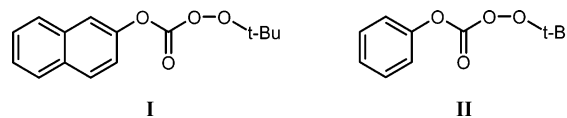
The ultrafast photofragmentation of arylperoxycarbonates R–O–C(O)O–O–*tert*-butyl (R = naphthyl, phenyl) is studied using femtosecond UV excitation at 266 nm and mid-infrared broadband probe pulses to elucidate the dissociation mechanism. Our experiments show that the rate of fragmentation is determined by the S₁-lifetime of the peroxide, i.e., the time constants of S₁ decay and of CO₂ and R–O• formation are identical. The fragmentation times are solvent dependent and for *tert*-butyl-2-naphthylperoxycarbonate (TBNC) vary from 25 ps in CH₂Cl₂ to 52 ps in *n*-heptane. In the case of the *tert*-butylphenylperoxycarbonate (TBPC) the decomposition takes 5.5 ps in CD₂Cl₂ and 12 ps in *n*-heptane. The CO₂ fragment is formed vibrationally hot with an excess energy of about 5000 cm⁻¹. The hot CO₂ spectra at high energy can be modeled assuming Boltzmann distributions with initial vibrational temperatures of ca. 2500 K which relax to ambient temperature with time constants of 280 ps in CCl₄ and 130 ps in *n*-heptane. In CCl₄ the relaxed spectra at 1.5 ns show 3.5% residual excitation in the *n* = 1 level of the asymmetric stretch vibration.

Introduction

Organic peroxides provide easy access to free radicals via facile O–O-bond cleavage and are used on a large scale as initiators in technical polymerization processes. They have been the subject of numerous studies, upon which rests much of the experimental basis of free radical chemistry.^{1,2} Their thermal fragmentation has been suggested to take place by either a stepwise or a concerted mechanism. In the former, initial O–O-bond cleavage in the peroxy compound R(O)CO–OR' is followed by subsequent decarboxylation of the R(O)CO• radical, whereas the latter involves a concerted two-bond cleavage yielding instantaneously R•, CO₂, and •OR'. While early trapping experiments established the existence of the benzoyloxy radical as an intermediate,³ Bartlett and co-workers showed in their pioneering work that the rate of thermal decomposition of a series of peroxyesters increases with the stability of the alkyl radical formed in their decarboxylation. This observation led them to suggest that concerted two-bond cleavage occurs whenever a sufficiently stable radical is formed, and that the intermediate R(O)CO• is not involved.⁴

As extremely short-lived intermediate aroyloxy radicals would not be detectable in thermolysis experiments, and because peroxyester photolysis “leads to chemical reactions that appear to mimic closely those of their...thermolyses”,⁵ Falvey and Schuster were led to carry out a landmark 266 nm picosecond laser flash photolysis experiment on *tert*-butyl-9-methylfluorene-9-percarboxylate (TBFP). They observed a first-order transient absorption rise with a time constant of 55 ps, which they attributed to the 9-methylfluorenyl radical formed by decarboxylation of the intermediate aroyloxy radical. They also pointed out that because of the very high stability of the

SCHEME 1: Investigated Compounds: *tert*-Butyl-2-naphthylperoxycarbonate (I; TBNC) and *tert*-Butylphenylperoxycarbonate (II, TBPC)



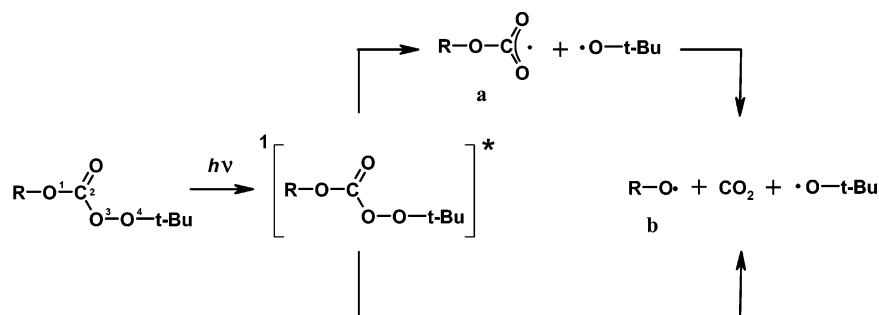
methylfluorenyl radical product, according to Bartlett's proposition this lifetime should represent something like a lower limit for aroyloxy radicals in general. As a consequence, the two-step mechanism would be the rule, with decarboxylation rates becoming very rapid for highly stable product radicals, but probably not exceeding $2 \times 10^{10} \text{ s}^{-1}$. This conclusion by Falvey and Schuster found support in subsequent photolysis studies showing that aroyloxy radicals generally decarboxylate on time scales ranging from roughly 50 ns to a few microseconds.^{6–11} It is also corroborated by recent observations of slow CO₂ production on a microsecond time scale in the photolysis of organic peroxides containing coumarin or bis(phenylethynyl)-benzene chromophores that indicate sequential fragmentation via intermediate carbonyloxy radicals.^{12,13}

However, in contradiction to this generally accepted view, measurements by picosecond UV-pump/IR-probe spectroscopy showed that in TBFP photolysis at 308 nm CO₂ appears within the experimental time resolution of about 2 ps.¹⁴ Instantaneous CO₂ formation was also observed following UV-photolysis of diarylperoxides, *tert*-butylbenzoylperoxide, and *tert*-butylphenylperoxycarbonate (TBPC; compound II in Scheme 1).^{15,16} This seemed to suggest that photodecomposition of these compounds via the electronically excited singlet state involves concerted bond cleavage without the intermediacy of an aroyloxy radical. On the other hand, a “slow” build-up of CO₂ with a time constant of 30 ps was found in the photolysis of *tert*-butyl-2-naphthylperoxycarbonate¹⁵ (TBNC; compound I in Scheme 1),

* Address correspondence to this author. E-mail: dschwar@gwdg.de.

[†] Max-Planck-Institut für Biophysikalische Chemie.

[‡] Universität Göttingen.

SCHEME 2: Sequential (top) and Concerted (bottom) Decomposition Path of Compounds I and II Following 266 nm Excitation to the (π,π^*) S_1 -State: (a) Aryloxy-carbonyloxy Radical and (b) Aryloxy Radical


which might be taken as evidence for fast sequential bond breakage on a time scale suggested by Falvey and Schuster for TBFP.

Evidently, the distinction between concerted and sequential reaction paths is intimately related to the time scale accessible to observation. A closer look at the “concerted” mechanism employing femtosecond pump–probe spectroscopy in the visible to near-IR spectral range led to the suggestion that in reality it consisted of an ultrafast sequence of elementary steps.^{17–21} According to this view, instantaneous O–O-bond scission generates vibrationally highly excited aryloxy radicals that may rapidly decarboxylate while they simultaneously undergo vibrational energy relaxation. The rate of CO₂ formation and aryloxy radical decay depends on the initial vibrational excess energy, the energy transfer efficiency, and the barrier height to decarboxylation. A quantitative model based on these assumptions and quantum chemical calculations (DFT B3LYP) could be successfully adjusted to reproduce the transient absorption data in the majority of systems studied, and it was concluded that the sequential mechanism is the prevalent mode of photofragmentation of organic peroxides.¹⁷

One has to bear in mind, however, that this analysis rests upon the correct assignment of transient spectra in the visible and near-IR. As spectral overlap of different absorption bands is extensive and spectral positions are known precisely for only a limited number of radicals and electronically excited states, their assignment to specific aryloxy radicals is difficult, in particular as on top of that there may be spectral shifts and band narrowing in the picosecond time range caused by vibrational cooling of hot intermediates. Therefore, it seems highly desirable to verify the fast sequential process by more reliably identifying radical intermediates using femtosecond broadband IR spectroscopy. For the purpose of this study we focus on the two peroxy-carbonates TBNC (**I**) and TBPC (**II**) previously characterized by different time constants of CO₂ formation, 30 ps¹⁵ and 2 ps,¹⁶ respectively. Similar time constants were also found in transient absorption decays in the near-IR region and assigned to the decarboxylation of the respective intermediate radicals **Ia** and **IIa** (see below).²⁰

The sequential and concerted photodecomposition paths of **I** and **II** that one wants to distinguish are depicted in Scheme 2. In recent quantum chemical calculations employing MP2 and DFT methods it was shown that the character of the R group and its influence on the heights of the relevant reaction barriers determines which pathway is the more favorable in thermolysis.²² The experimental findings so far seem to indicate that for both **I** and **II** the sequential pathway is dominant and that the time scales of intermediate radical decay differ by a factor of 10.

Experimental Technique

Pump and probe pulses were generated from the output of a home-built Ti:sapphire oscillator/regenerative amplifier system producing 100 fs laser pulses at a repetition rate of 1 kHz with energies of 750 μ J centered at 800 nm. Part of the energy was used to produce 267 nm pump pulses by frequency doubling and subsequent mixing of generated 400 nm with remaining 800 nm light in two BBO crystals. The UV light was attenuated to pulse energies of 0.5–2 μ J and focused with a 200 mm focal length quartz lens down to a spot size of 400 μ m at the sample. 250 μ J of the regenerative amplifier output was used to pump a continuum seeded BBO based collinear optical parametric amplifier, which after difference frequency mixing of signal and idler provided mid-IR pulses with typical energies of 0.5–1 μ J and a bandwidth of 200 cm⁻¹.²³ The IR light was split into a probe and a reference beam by means of a CaF₂ wedge. Both pulses were focused into the sample cell, whereby the probe pulse was overlapped with the pump. After passing the cell probe and reference beam were spectrally dispersed in a grating spectrometer and independently imaged on a liquid nitrogen cooled HgCdTe detector (2 × 32 pixels) with 11.4 nm resolution.

A computer-controlled translation stage adjusted the time delay between pump and probe pulses. The relative plane of polarization of both pulses was adjusted to 54.7° to avoid signal contributions arising from rotational relaxation. Every second pump pulse was blocked by a synchronized chopper to measure long-term drifts of the background absorption. To avoid spectral and temporal distortion of the mid-IR pulses by CO₂ and water absorption in air the pump–probe setup was purged with dry nitrogen.

The measurements were performed in a stainless steel flow cell equipped with CaF₂ windows of 1 mm thickness. The optical path length inside the cell varied between 0.6 and 1.0 mm. Concentrations of peroxyesters were adjusted so that the optical density of the sample at the pump wavelength was about 1.

The peroxyesters were synthesized in our laboratory by reaction of sodium *tert*-butyl peroxide with chloroformic acid phenyl ester and chloroformic acid 2-naphthyl ester, respectively.²⁴ After column chromatography the purity of peroxyesters was >95% as controlled by ¹H NMR spectroscopy. Perdeuterated solvents acetonitrile (MeCN-*d*₃) and dichloromethane (CH₂D₂) were obtained from Deutero GmbH (99.6% deuteration grade). Tetrachloromethane (CCl₄) and *n*-heptane were purchased from Merck (p.a.). All experiments were performed at room temperature.

The experimental studies were accompanied by density functional theory (DFT) calculations performed with the Gaussian03 software package²⁵ to verify the structural and vibrational

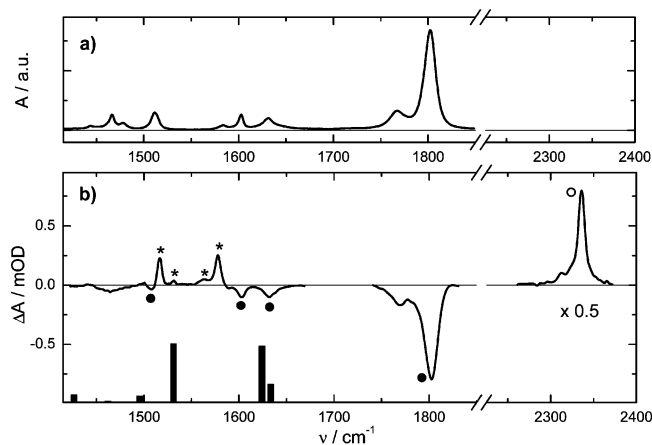


Figure 1. (a) Linear absorption spectrum of **I** in MeCN- d_3 ; (b) transient spectrum 1.3 ns after 267 nm excitation of **I** in MeCN- d_3 (at 2220–2370 cm^{-1} the spectrum was recorded in CCl_4 because MeCN- d_3 is opaque in this range); (●) bleaching of **I**; (○) formation of CO_2 ; (*) formation of **Ib**; black bars indicate calculated frequencies and relative intensities of **Ib**.

properties of the investigated compound. For the peroxides we used the B3LYP functional in conjunction with a 6-31G(d,p) basis set. Product radicals were computed with the UB3LYP functional and a cc-pVTZ basis set.

Results

1. TBNC (I). In Figure 1b a transient IR spectrum recorded 1.3 ns after UV excitation of **I** in MeCN- d_3 is compared with the corresponding linear absorption spectrum (Figure 1a). Because of the 32-pixel resolution of the HgCdTe detector and the limited bandwidth of the IR probe pulse the transient spectrum of Figure 1b was constructed from seven individual overlapping narrow-band spectra in the range 1400–1850 cm^{-1} . At 2220–2370 cm^{-1} the transient was recorded in CCl_4 since MeCN- d_3 is opaque in this range. We estimate the error of the relative amplitude of spectral features arising from this procedure to be <25%.

The transient spectrum of Figure 1b shows four prominent negative peaks marked by full circles representing direct mirror images of the linear spectrum in the upper panel and indicating photobleaching of **I**. Most prominent is the CO stretch vibration at 1802 cm^{-1} with a secondary peak at 1767 cm^{-1} . The FTIR spectrum of crystalline **I** in a KBr pellet shows only a single peak centered at 1792 cm^{-1} suggesting the presence of different conformers of **I** in solution with different CO stretch resonances. DFT calculations reveal a dominant influence of the configuration of the $\text{O}^1\text{—C}^2\text{—O}^3\text{—O}^4$ moiety (see Scheme 2) on the CO stretch frequency. According to these calculations we attribute the stronger blue-shifted absorption to the trans-isomer whereas the weaker band is assigned to the slightly less stable (180 cm^{-1}) cis-isomer.

The strongest line appearing in the transient spectrum is the asymmetric stretch vibration of newly formed CO_2 at 2336 cm^{-1} (open circle in Figure 1b; amplitude scaled by a factor of 0.5). Additionally, four weaker absorptions at 1518, 1531, 1560, and 1577 cm^{-1} (asterisks) are detected which we attribute to the 2-naphthyloxy radical **Ib**. Infrared spectra of this radical have not been published so far. Our DFT calculations of the radical **Ib** provide two weak and two intense vibrations in this frequency range (see the black bars in Figure 1b) in nice agreement with the measured spectrum. The strong 1518 cm^{-1} peak (calculated: 1532 cm^{-1} (without correction factor), integrated intensity

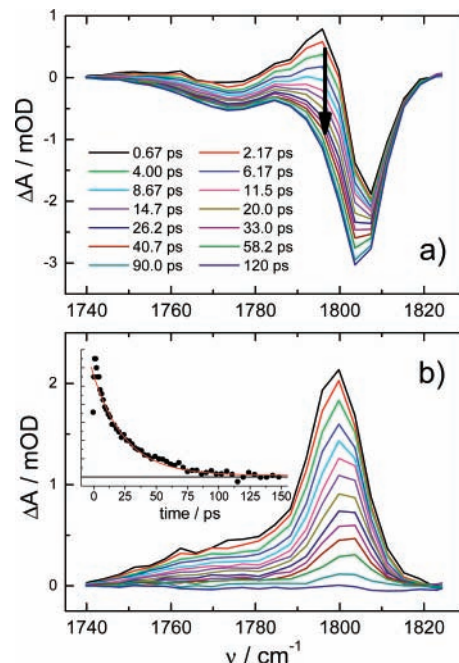


Figure 2. (a) Transient spectra of the CO stretch absorption band of **I** in CCl_4 recorded at selected pump–probe delay times; (b) evolution of the excited state CO stretching band derived from the difference between the transients of part a and the spectrum at 150 ps pump–probe delay (color code is the same as for the upper panel); the insert shows the decay of the integrated band intensity (exponential fit gives a time constant of 25 ± 2 ps).

$I = 41.7$ km/mol) can be assigned to the CO stretch, and the band at 1577 cm^{-1} (calculated: 1624 cm^{-1} , $I = 40.1$ km/mol) is of CC ring stretch character.

For selected peaks of Figure 1b the spectral and temporal evolution is presented in Figures 2–5. Immediately upon excitation by the UV pump pulse, CO stretching bands in the electronic ground state and the lowest excited singlet state appear as bleach and absorption, respectively, as shown in Figure 2a for **I** in CCl_4 . With increasing pump–probe delay the excited state population decays, photoproducts are formed, and only the ground state bleach remains at long times. Spectra of the CO stretching band in the excited state are obtained separately by subtracting the ground state bleach, using the transient at 150 ps. As shown in Figure 2b this band peaks at a lower frequency (1799 cm^{-1}) than in the ground state (1806 cm^{-1}). From the decay of the integrated band intensity (insert in Figure 2b) the S_1 lifetime of 25 ± 2 ps is obtained by exponential fitting. The analysis of the temporal evolution of the carbonyl stretch band also indicates that the electronic ground state is not repopulated on the time scale of the experiment up to 1.5 ns. In addition, in the frequency window accessed in our experiment there is no transient absorption that could be assigned to the CO band in other excited electronic states. One may, therefore, conclude that the quantum yield of photofragmentation has to be close to unity. We find no evidence that the quantum yield is affected by competing intersystem crossing to the triplet state of **I**.

Figure 3 shows the formation of CO_2 monitored at the ν_3 asymmetric stretch absorption band after photoexcitation of **I** in CCl_4 . The contour diagram demonstrates that initially the spectrum is broad and red-shifted with respect to the band origin of the $(0,0,0) \rightarrow (0,0,1)$ transition at 2336 cm^{-1} . With time the spectrum narrows and its intensity at 2336 cm^{-1} increases simultaneously. This behavior has been observed in earlier studies^{15,16} and can be attributed to the formation of vibrationally

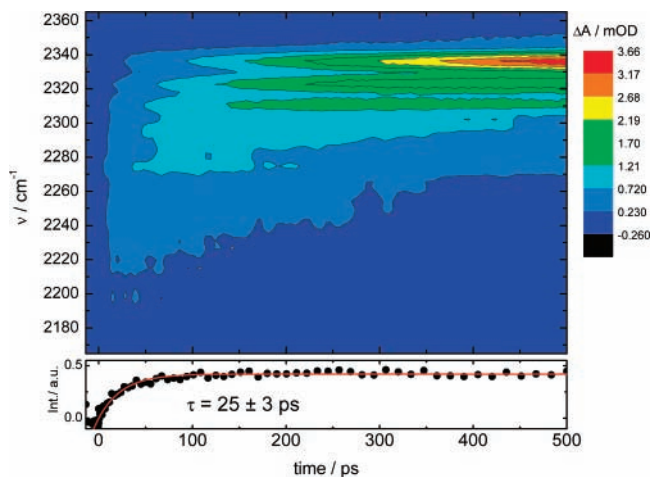


Figure 3. Spectral evolution of the ν_3 absorption band of CO_2 produced in the photodissociation of **I** in CCl_4 . The lower panel shows the integrated band intensity (red curve: exponential fit to the data with time constant of 25 ± 3 ps).

hot CO_2 cooling down by vibrational energy transfer to the surrounding medium. However, due to higher spectral resolution and better signal-to-noise ratio, in Figure 3 we can identify a 12.5 cm^{-1} modulation on top of the bands that is seen more clearly at individual spectra for selected pump–probe delays in Figure 4. The temporal evolution of the CO_2 concentration is derived by evaluating the integral absorbance of the bands. The corresponding time-dependence is shown in the lower panel of Figure 3. Exponential fitting gives a characteristic CO_2 build-up time of 25 ± 3 ps.

The formation of the 2-naphthyloxy radical **Ib** after UV excitation of **I** in CD_2Cl_2 is presented in Figure 5. At early times only a weak bleaching arising from the superposition of ground state bleach and excited state absorption of **I** is observed in the transient spectrum of Figure 5b (the stationary spectrum of **I** is shown for comparison in Figure 5a). Subsequently, an absorption peak at 1519 cm^{-1} with a satellite at 1526 cm^{-1} emerges. The formation time of this feature derived from the integrated band intensity (Figure 5c) is 26 ± 3 ps. The same time constant was found for the band at 1577 cm^{-1} .

The kinetic data for the photoinduced decomposition of **I** are summarized in Table 1. Within experimental error of about 10% the time constants of S_1 decay of the peroxide observed at its carbonyl absorption band agree with the formation time of CO_2 or the spectral features marked by asterisks in Figure 1. Consequently, the transient absorptions in the $1510\text{--}1590 \text{ cm}^{-1}$ range of Figures 1 and 5 are attributed to the 2-naphthyloxy radical **Ib**. Our data provide no evidence for the appearance of an intermediate naphthyloxy carbonyloxy radical **Ia**.

The *tert*-butoxy radical is invisible to us because in a difference spectrum only those vibrations are detectable which change their frequency and/or intensity. For the *tert*-butoxy radical this is mainly the case for the CO stretch vibration, whereas C–H stretch and bend will not be changed significantly with respect to the parent molecule. According to literature²⁶ the CO stretch vibration of alkyloxy radicals is outside our experimental window at around 1000 cm^{-1} .

2. TBPC (II). In Figure 6 the linear IR spectrum (a) of **II** is compared with its transient absorption spectrum measured 1.3 ns after UV-photoexcitation (b). The transient spectrum was generated in the same manner as described for Figure 1b. At $2230\text{--}2390 \text{ cm}^{-1}$ the buildup of the CO_2 asymmetric stretch band was measured in *n*-heptane since $\text{MeCN-}d_3$ is opaque in this frequency range. Note that the band is considerably broader

than in CCl_4 (Figure 1b). In Figure 6b one can identify four negative peaks assigned by full circles representing photo-bleaching of the parent molecule **II**. Three transient absorption peaks marked by asterisks indicate formation of the phenyloxy radical **Ib**. The vibrational frequencies at 1490 , 1512 , and 1549 cm^{-1} are in excellent agreement with those found for **Ib** in low-temperature argon matrices (1481 , 1515 , and 1550 cm^{-1}) and were assigned to CO stretch, combination of CC stretch and CH bend, and CC ring stretch modes, respectively.²⁷

For a given solvent, the formation of the photoproducts CO_2 and **Ib** and the decay of the excited parent molecule can be characterized by a single time constant. As an example we show in Figure 7 the temporal evolution of the carbonyl stretch band of **II** in $\text{MeCN-}d_3$ after UV excitation. At early times a superposition of ground state bleach and excited state absorption is observed in Figure 7a (similar to the naphthyl compound in Figure 2). At later times, when the S_1 state of **II** is depopulated, only the ground state bleach remains. The time constant of the S_1 decay is evaluated from a plot of the integrated band intensity vs time (insert in Figure 7a) to be 6 ± 1 ps. The excited state spectra were calculated separately by subtracting the ground state bleach at 30 ps. The corresponding spectra are presented in Figure 7b and are 2 cm^{-1} red-shifted with respect to the ground state spectrum. Obviously, the oscillator strength is about a factor of 2 larger for the excited than for the ground state. Also in this case, following the same arguments as above, the photofragmentation quantum yield is practically unity.

The kinetic data for the photodissociation of **II** are summarized in Table 2. The time constants of S_1 decay and CO_2 and phenyloxy radical formation are almost identical. The phenyloxy carbonyloxy radical **Ia** cannot be detected.

Discussion

1. Decomposition Mechanism. The essential observations regarding the peroxide photofragmentation mechanism may be summarized as follows:

- (1) Instantaneous bleaching of the ground state CO stretch band is matched by the instantaneous appearance of corresponding slightly red-shifted CO stretch absorption in the S_1 -state of the parent peroxide.
- (2) Subsequent formation and decay of transient IR bands are governed by a single time constant.
- (3) Appearing absorption bands can be assigned to product radicals and CO_2 . Transient bands that could be assigned to aryloxy carbonyloxy radicals (**Ia**, **IIa**) were not found.

The time constant of 25 ps found for TBNC (**I**) agrees well with those measured earlier by different techniques.^{15,20} In contrast to previous interpretations of this observation, however, our findings strongly suggest that sequential bond cleavage to produce an intermediate **Ia**, be it highly vibrationally excited or vibrationally cold, does not take place on this time scale. This implies that the previous assignment of the transient absorption band in the near-IR region to this radical has to be erroneous.²⁰ In view of the present study it has to be reassigned to the $S_n \leftarrow S_1$ transition of TBNC. To maintain the previous interpretation one would have to assume that the slightly red-shifted instantaneous transient CO stretch absorption band belongs to **Ia**. As discussed above, experimental and theoretical evidence clearly shows that this would not be a reasonable assignment. In addition, we measured the fluorescence lifetime of TBNC in *n*-heptane to be 51 ps, providing further support for our new assignment. Of course, one cannot rule out an ultrafast sequence of bond scissions, in which the O–O bond is broken first with a rate constant of $(25 \text{ ps})^{-1}$, followed by

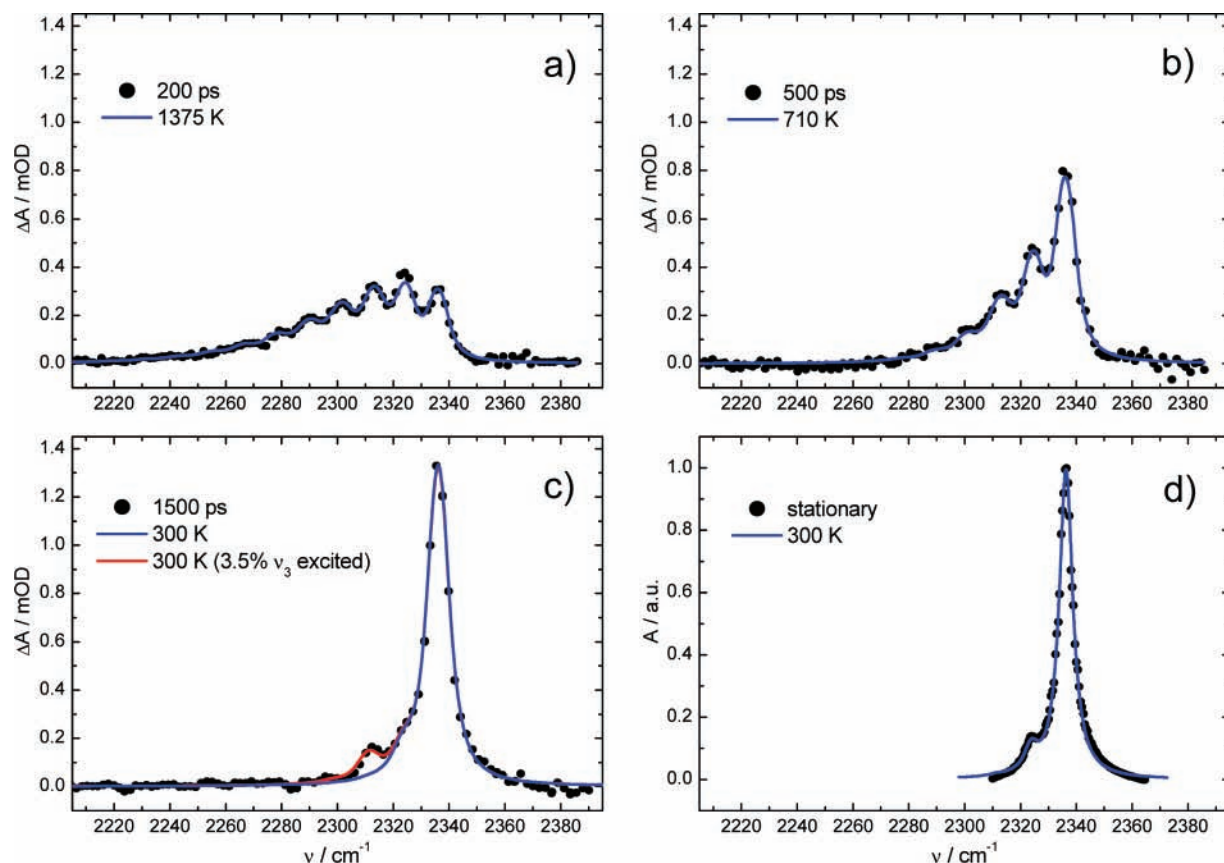


Figure 4. (a–c) Transient spectra of the ν_3 absorption band of CO_2 at selected pump–probe time delays formed after decomposition of **I** in CCl_4 (each spectrum is composed of 4 individual spectra offset by 3 nm); (d) linear absorption spectrum of CO_2 dissolved in CCl_4 ; lines are simulated thermal spectra (see text).

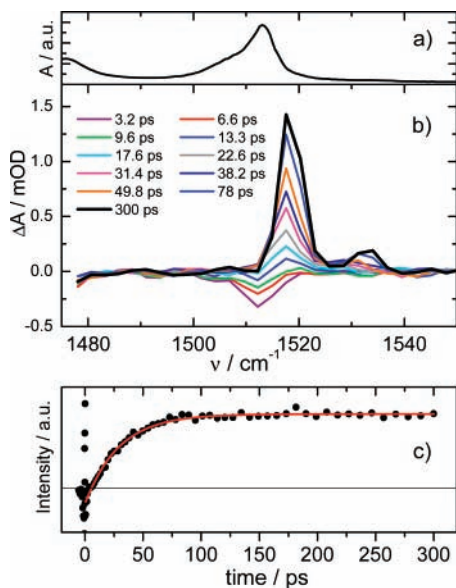


Figure 5. Formation of **Ib** after photodissociation of **I** in CD_2Cl_2 : (a) linear absorption spectrum of **I** in CD_2Cl_2 ; (b) the emerging strong absorption band is attributed to the CO-stretch vibration of **Ib**; (c) integrated band intensity (red curve: exponential fit to the data with time constant of 25 ± 3 ps).

O–C bond cleavage at an order of magnitude faster rate. This kind of intermediacy of an extremely unstable **Ia** would still be compatible with our measurements. For TBPC (**II**) the situation is identical, the only difference being that photofragmentation via the S_1 -state is much faster. Again, previous assignments of transients in the near-IR²⁰ have to be corrected,

TABLE 1: Time Constants (in ps) Observed for the Photodissociation of **I by fs-IR (this work, ref 15), ps-VIS–Pump–Probe Spectroscopy (ref 20), and Fluorimetry (*, this work)**

| solvent | S_1 -lifetime of I | formation of CO_2 | formation of Ib |
|--------------------------|---|-------------------------------|------------------------|
| CCl_4 | 25 ± 2 27 ± 5^{20} | 25 ± 3 31 ± 5^{15} | |
| propylene carbonate | 25 ± 1^{20} | | 19 ± 5^{20} |
| CD_2Cl_2 | 25 ± 2 | | 26 ± 3 |
| $\text{MeCN-}d_3$ | 25 ± 3 | | 26 ± 3 |
| MeCN | 36 ± 2^{20} | | |
| CH_3OH | 31 ± 2^{20} | | |
| <i>n</i> -heptane | 52 ± 3 $51 \pm 1^*$ 41 ± 5^{20} | 55 ± 5 | |

and there is no evidence for an intermediate **Ia** with a lifetime longer than about 100 fs in this case. We think, therefore, that from the point of view of photochemical kinetics the mechanism in both cases may be considered as concerted. The question whether both bonds break synchronously cannot be answered on the basis of these experiments.

From a thermodynamic point of view the fact that photofragmentation is faster for **II** than for **I** might look surprising, as **Ib** is the more stable product radical compared to **Ib**. Similarly, assuming that the rate-controlling step of the overall fragmentation sequence is S_0 – S_1 internal conversion from the equilibrated S_1 -state, the energy gap law also does not provide a reasonable explanation since the S_0 – S_1 energy gap is smaller for **I**. On the other hand, because of the higher density of educt states, the statistical rate coefficient for unimolecular fragmentation from the S_1 -state would be expected to be significantly smaller for **I**. Considering the 25–50 ps time scale for the

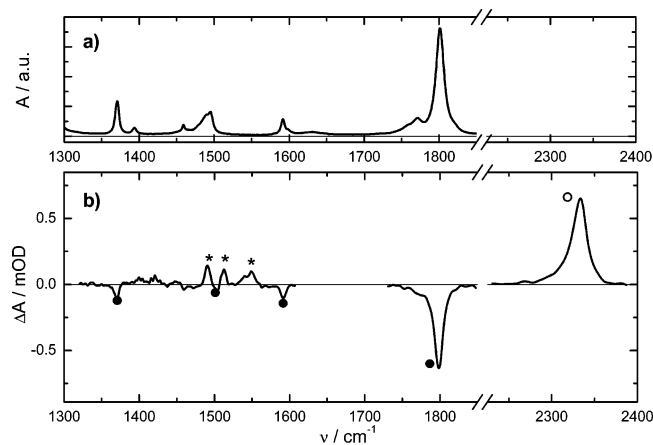


Figure 6. (a) Linear absorption spectrum of **II** in MeCN- d_3 ; (b) transient spectrum 1.3 ns after 267 nm excitation of **II** in MeCN- d_3 at 2220–2390 cm^{-1} the spectrum was recorded in *n*-heptane because MeCN- d_3 is opaque in this range; (●) bleaching of **II**; (○) formation of CO_2 ; and (*) formation of **IIb**.

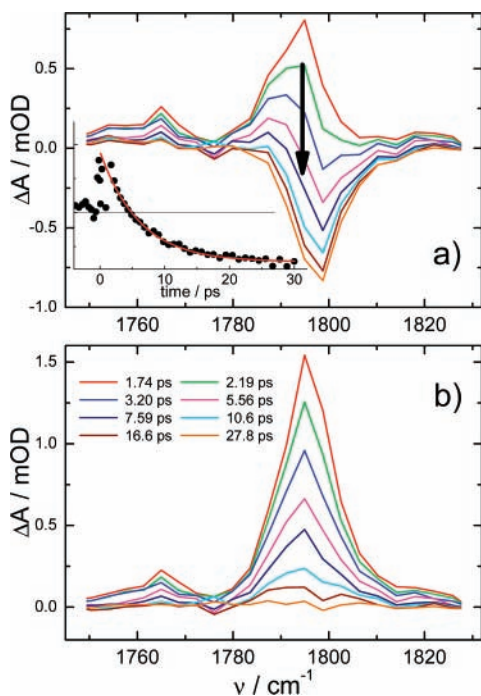


Figure 7. (a) Transient spectra of the CO stretch absorption band of **II** in MeCN- d_3 recorded at selected pump–probe delay times; the insert shows the decay of the integrated band intensity (exponential fit gives a time constant of 6.0 ± 1.0 ps); (b) evolution of the excited state CO stretching band derived from the difference between the transients of part a and the spectrum at 30 ps pump–probe delay (color code is the same for both panels).

photofragmentation of **I**, a statistical description of the reaction rate most probably would be valid, while for the ultrafast dissociation of **II** such an approach might be questionable, but still a nonstatistical reaction of **II** would be even faster. It appears, therefore, that photofragmentation occurs on the S_1 potential energy surface and does not involve internal conversion to the ground state surface. At present, without detailed knowledge about the excited state potential energy surface, a quantitative explanation is still lacking. For the same reason, a discussion of the solvent effect—slowing down of the fragmentation rate in *n*-heptane by about a factor of 2—has to remain qualitative. If one takes into account also the time constants

TABLE 2: Time Constants (in ps) Observed for the Photodissociation of **II by fs-IR (this work, ref 16) and ps-VIS–Pump–Probe Spectroscopy (ref 20)**

| solvent | S_1 -lifetime of II | formation of CO_2 | formation of IIb |
|--------------------------|------------------------------|----------------------------|-------------------------|
| CD_2Cl_2 | 5.5 ± 1.0 | | |
| CH_2Cl_2 | | | |
| propylene carbonate | 5.9 ± 0.6^{20} | $< 10^{16}$ | |
| MeCN- d_3 | 6.0 ± 1.0 | | 5.5 ± 1.0 |
| MeCN | 6.3 ± 0.6^{20} | | |
| <i>n</i> -heptane | 12 ± 3 | 12 ± 3 | |
| | 13 ± 2^{20} | | |

obtained earlier in the visible spectral range shown in Table 2, there seems to be no clear trend, neither with solvent polarity nor with viscosity. But these data may suffer from overlapping photoproduct transients that obscure the picture. One may observe that the electronic polarizability of *n*-heptane as measured by $(n^2 - 1)/(n^2 + 1)$ is smaller by about 15% than that of CCl_4 and CH_2Cl_2 . If one assumes that there is a barrier along the reaction path resulting from an intersection of two harmonic surfaces which show a linear relative energy shift with solvent polarizability, the barrier height would change appreciably and could account for the observed change in rate coefficient. Acetonitrile, though, has a refractive index slightly smaller than that of *n*-heptane, but on the other hand it is strongly polar with ultrafast dielectric relaxation components which could contribute to the lowering of relevant regions of the potential energy surface even on the time scale of a fragmentation. At present, however, we do not know whether the photofragmentation is a barrier-controlled process. Investigations of the temperature dependence could help to clarify this point.

2. Modeling of CO_2 Spectra. In a previous paper the spectral evolution of the ν_3 asymmetric stretch absorption band of CO_2 produced in the UV-induced decomposition of aromatic peroxides was attributed to vibrational cooling of the initially excited molecule.¹⁶ The excess energy originates from the energy release associated with the structural relaxation of the bent OCO moiety to form the linear CO_2 molecule. By using an anharmonic oscillator model²⁸ it was possible to assign vibrational temperatures T to the hot spectra and calculate the temperature as a function of time. However, spectral resolution in this earlier work was limited to 12 cm^{-1} such that the modulation shown in Figure 4 was not resolved. Therefore, we expect to get a more accurate and complete picture of the vibrational relaxation process when analyzing our data using the same procedure.

The broadening of the CO_2 ν_3 -band upon vibrational excitation originates from anharmonic coupling among symmetric stretch (ν_1), bend (ν_2), and the asymmetric stretch modes. According to the model of Hamm et al.²⁸ the spectrum $A_3(\tilde{\omega})$ of the asymmetric stretch mode is given by

$$A_3(\tilde{\omega}) = \sum_{n_3=0}^S \{ [a(n_3) - a(n_3 + 1)](n_3 + 1) \times \sum_{n_1=0}^S \sum_{n_2=0}^S a(n_1)a(n_2) \cdot L[\tilde{\omega} - \tilde{\nu}(n_3 \rightarrow n_3 + 1)] \} \quad (1)$$

where $a(n_k)$ is the relative population in the n th level of mode k , $L(\tilde{\omega})$ is a line shape function, and S is the maximum number of vibrational levels considered in the calculations. For our calculations we used $S = 6$ for ν_3 , $S = 10$ for ν_1 , and $S = 15$ for ν_2 . The location of a spectral line for a transition $n_3 \rightarrow n_3 +$

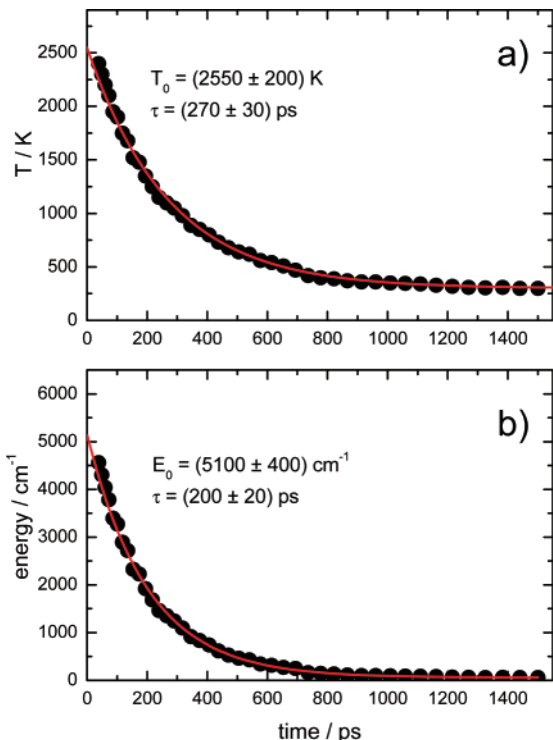


Figure 8. Temporal evolution of the vibrational temperature (a) and the energy (b) of CO₂ produced after photodissociation of **I** in CCl₄.

1 of mode ν_3 coupled to the other modes is given by

$$\tilde{\nu}(n_3 \rightarrow n_3 + 1) = \tilde{\omega}_3 + 2x_{33} + \frac{x_{13} + x_{23}}{2} + 2x_{33}n_3 + x_{13}n_1 + x_{23}n_2 \quad (2)$$

In the gas phase the harmonic frequency of the asymmetric stretch vibration is $\tilde{\omega}_3 = 2396.30 \text{ cm}^{-1}$.²⁹ The anharmonicity constants³⁰ $x_{33} = -12.50 \text{ cm}^{-1}$, $x_{13} = -19.27 \text{ cm}^{-1}$, and $x_{23} = -12.51 \text{ cm}^{-1}$ are all negative indicating a red shift of the ν_3 band when CO₂ is vibrationally excited.

The populations $a(n)$ in eq 1 are normalized for each mode and are assumed to be Boltzmann distributed, i.e.,

$$a(n) = \frac{g_n \exp(-n\hbar\omega/k_B T)}{\sum_n g_n \exp(-n\hbar\omega/k_B T)} \quad (3)$$

where ω is the fundamental frequency of the vibrational mode. The degeneracy of $g_n = n + 1$ has to be taken into account for the bend vibration.

At first eq 1 was fitted to the room temperature spectrum of CO₂ dissolved in CCl₄ as presented in Figure 4d by the blue line. Almost perfect agreement to the FTIR spectrum is obtained by using a Lorentzian line shape of 6.0 cm^{-1} width (fwhm). The position of the main peak at 2336 cm^{-1} representing the $(0,0,0) \rightarrow (0,0,1)$ transition is red-shifted with respect to the gas phase. This is taken into account by reducing the harmonic frequency $\tilde{\omega}_3$ in eq 2 by 19.4 cm^{-1} . The satellite at 2324 cm^{-1} is due to the $(0,1,0) \rightarrow (0,1,1)$ transition and reflects 7.5% excitation of the bend vibration at 300 K. Its shift relative to the main peak is determined by the nondiagonal anharmonic term x_{23} in eq 2.

For the calculation of transient CO₂ spectra the line shape was assumed to be temperature independent. The spectrometer resolution (given by the pixel width of the HgCdTe-detector)

TABLE 3: Initial Vibrational Temperatures T , Temperature τ_T , and Energy Decay Time Constants τ_e of CO₂ Produced from Peroxide Photodissociation

| compd | T/K | solvent | τ_T/ps | τ_e/ps |
|-----------|----------------|---------------------------------|--------------------|--------------------|
| I | 2550 ± 200 | CCl ₄ | 270 ± 30 | 200 ± 20 |
| | 2600^{16} | n-heptane | 140 ± 20 | 110 ± 20 |
| II | 2500 ± 200 | CH ₂ Cl ₂ | 67 ± 5^{16} | 51 ± 4^{32} |
| | 2700^{16} | | | |

of 6 cm^{-1} at this frequency range was taken into account by using an effective line shape function computed from the convolution of a Lorentzian and a rectangular function each of 6 cm^{-1} width. Parts a–c of Figure 4 show good agreement between measured and calculated spectra. The 12.5 cm^{-1} progressions seen on top of the hot spectra represent direct images of the population of the bend vibration in the individual quantum states. Note that apart from an amplitude factor the only adjustable parameter in the fitted spectra is the temperature, which is evaluated as a function of time and plotted in Figure 8a. The initial CO₂ vibrational temperature after photodecomposition of **I** is $2550 \pm 200 \text{ K}$. The temperature decay has a characteristic time constant of $270 \pm 30 \text{ ps}$ in CCl₄ and is translated into an energy vs time curve according to

$$E(T) = \frac{\hbar\omega_i}{\sum_i 1 - \exp(-\hbar\omega_i/k_B T)} \quad (4)$$

where the summation is over the CO₂ vibrational modes with frequency ω_i (the degenerate bend vibration is counted twice). Due to the high nonlinearity of $E(T)$ the time constant of the vibrational energy decay of CO₂ is considerably faster ($200 \pm 20 \text{ ps}$, see Figure 8b) than the temperature decay. The results of CO₂ energy relaxation are summarized in Table 3. A closer look at Figure 4c reveals that the CO₂ spectrum measured at a pump probe delay of 1.5 ns cannot be fitted by a thermal spectrum. Considering the time constants of $T(t)$ or $E(t)$ evaluated from the initial decay of both quantities the CO₂ molecule must be thermalized at 300 K by this time. The corresponding simulated spectrum (blue line), however, does not account for a small peak 25 cm^{-1} red-shifted from the $(0,0,0) \rightarrow (0,0,1)$ transition. Bend excitation cannot be responsible for this peak because that would require a population inversion with $a(2) > a(1)$, a situation obviously not observed at earlier times. Therefore, we attribute this peak to residual population in the $n = 1$ level of the asymmetric stretch vibration: 3.5% excitation of ν_3 in $n = 1$ yields excellent agreement between simulated (red curve in Figure 4c) and experimental spectra.

Recent molecular dynamics calculations of CO₂ vibrational relaxation produced in the photodissociation of organic peroxides have shown^{31,32} that the different modes lose their energy on different time scales. Whereas symmetric stretch and bend vibrations are strongly coupled due to Fermi resonance and jointly relax with a time constant of 210 ps^{31} in CCl₄, the high-frequency asymmetric stretch is only weakly coupled to the other modes and relaxes on much longer time scales. While this result obviously is in agreement with the nonthermal spectrum in Figure 4c, the origin of the excess energy in ν_3 has to be clarified. One possibility is that it originates (as for the bend) from the energy release associated with the restructuring of the OCO moiety after bond breakage to form the linear CO₂. This would require a precursor where initially the two CO bonds are of different length. The latter could be the case for the parent peroxide and a hypothetical intermediate (CO)–O–O–*t*-Bu, but not for radical **a** in Scheme 1. For energetic reasons,

however, it is unlikely that ArO–C bond breakage occurs prior to O–O bond scission. Hence a reaction mechanism may operate in which the ArO–C and O–O bonds break synchronously, such that the excess energy in ν_3 would be a signature of the asymmetric structure of the OCO moiety in the peroxide.

Alternatively, the ν_3 excitation could be caused by weak anharmonic coupling of the asymmetric stretch to the other modes, which is enhanced at high vibrational energy. This might be sufficient to populate $\nu_3(n=1)$ to some extent before vibrational relaxation takes place, even if ν_3 is not directly excited in the process of dissociation. As ν_1 and ν_2 transfer their energy to the bath, coupling to ν_3 reduces and 3.5% of the population remains trapped in its $n = 1$ level. This mechanism is supported by our molecular dynamics simulations. Figures 2 and 4 of ref 32 demonstrate that directly after excitation of ν_1 and ν_2 there is a short period of several tens of picoseconds where the ν_3 energy slowly increases. When during vibrational relaxation symmetric stretch and bend mode lose their energy and reach a threshold of about 4000 cm^{-1} the energy in ν_3 becomes constant at a few hundred wavenumbers above thermal energies. No further temporal evolution in ν_3 is observed up to 1 ns.

On the basis of the present results, a definite conclusion regarding the mechanism leading to excitation of the asymmetric stretch mode cannot be reached. Further experimental and theoretical studies are underway to clarify this point, as it concerns an important basic aspect of the photofragmentation dynamics.

Conclusions

In the present work we have studied the photodissociation mechanism of the arylperoxycarbonates TBNC (**I**) and TBPC (**II**) by means of ultrafast infrared spectroscopy. By monitoring the temporal evolution of vibrational marker bands it is shown that after UV excitation the S_1 states of both peroxides decay with the same respective rate as the final products CO_2 and carbonyloxy radical are formed. A previously proposed sequential dissociation mechanism with subpicosecond O–O bond breakage and a spectroscopically accessible intermediate arylloxycarbonyloxy radical can be ruled out.

The high initial vibrational energy of the CO_2 fragment results from the structural relaxation of the bend O–C–O moiety after bond breakage. Whether the 3.5% residual excitation in the $n = 1$ level of the asymmetric stretch vibration observed in CCl_4 at 1.3 ns is also due to this structural relaxation or caused by anharmonic coupling with symmetric stretch and bend vibration at high energies cannot be clarified at this stage. Here additional experiments with peroxides releasing CO_2 with less vibrational excess energy¹⁶ are required.

Acknowledgment. The authors are grateful to Jens Schimpfhauser and Jürgen Bienert for the preparation and purification of the investigated compounds. We thank Klaas Zachariasse and Sergey Druzhinin for performing fluorescence lifetime measurements on TBNC. We also thank Jürgen Troe for continuous support of this work.

References and Notes

- (1) Fujimori, K. In *Organic Peroxides*; Ando, W., Ed.; Wiley: New York, 1992; p 319.
- (2) Sawaki, Y. In *Organic Peroxides*; Ando, W., Ed.; Wiley: New York, 1992; p 425.
- (3) Hammond, G. G.; Soffer, L. M. *J. Am. Chem. Soc.* **1950**, *72*.
- (4) Bartlett, P. D.; Hiatt, R. R. *J. Am. Chem. Soc.* **1958**, *80*, 1398.
- (5) Falvey, D. E.; Schuster, G. B. *J. Am. Chem. Soc.* **1986**, *108*, 7419.
- (6) Misawa, H.; Sawabe, K.; Takahara, S.; Sakuragi, H.; Tokumaru, K. *Chem. Lett.* **1988**, 357.
- (7) Chateaufneuf, J.; Luszyk, J.; Ingold, K. U. *J. Am. Chem. Soc.* **1988**, *110*, 2877.
- (8) Chateaufneuf, J.; Luszyk, J.; Ingold, K. U. *J. Am. Chem. Soc.* **1988**, *110*, 2886.
- (9) Wang, J.; Tateno, T.; Sakuragi, H.; Tokumaru, K. *J. Photochem. Photobiol. A* **1995**, *92*, 53.
- (10) Wang, J.; Itoh, H.; Tsuchiya, M.; Tokumaru, K.; Sakuragi, H. *Tetrahedron* **1995**, *51*, 11967.
- (11) Najiwaru, T.; Hashimoto, J.; Segawa, K.; Sakuragi, H. *Bull. Chem. Soc. Jap.* **2003**, *76*, 575.
- (12) Polyansky, D. E.; Neckers, D. C. *J. Phys. Chem. A* **2005**, *109*, 2793.
- (13) Polyansky, D. E.; Danilov, E. O.; Voskresensky, S. V.; Rodgers, M. A. J.; Neckers, D. C. *J. Phys. Chem. A* **2006**, *110*, 4969.
- (14) Aschenbrücker, J.; Steegmüller, U.; Buback, M.; Ernsting, N. P.; Schroeder, J. *J. Phys. Chem. B* **1998**, *102*, 5552.
- (15) Aschenbrücker, J.; Steegmüller, U.; Buback, M.; Ernsting, N. P.; Schroeder, J. *Ber. Bunsenges. Phys. Chem.* **1998**, *102*, 965.
- (16) Buback, M.; Kling, M.; Seidel, M. T.; Schott, F. D.; Schroeder, J.; Steegmüller, U. *Z. Phys. Chem.* **2001**, *215*, 717.
- (17) Buback, M.; Kling, M.; Schmatz, S.; Schroeder, J. *Phys. Chem. Chem. Phys.* **2004**, *6*, 5441.
- (18) Abel, B.; Assmann, J.; Buback, M.; Kling, M.; Schmatz, S.; Schroeder, J. *Angew. Chem., Int. Ed.* **2003**, *42*, 299.
- (19) Abel, B.; Assmann, J.; Botschwina, P.; Buback, M.; Kling, M.; Oswald, R.; Schmatz, S.; Schroeder, J.; Witte, T. *J. Phys. Chem. A* **2003**, *107*, 5157.
- (20) Abel, B.; Assmann, J.; Buback, M.; Grimm, C.; Schmatz, S.; Schroeder, J.; Witte, T. *J. Phys. Chem. A* **2003**, *107*, 9499.
- (21) Abel, B.; Buback, M.; Kling, M.; Schmatz, S.; Schroeder, J. *J. Am. Chem. Soc.* **2003**, *125*, 13274.
- (22) Gu, Z. H.; Wang, Y. X.; Balbuena, P. B. *J. Phys. Chem. A* **2006**, *110*, 2448.
- (23) Hamm, P.; Kaindl, R. A.; Stenger, J. *Opt. Lett.* **2000**, *25*, 1798.
- (24) Lorand, J. P.; Bartlett, P. D. *J. Am. Chem. Soc.* **1966**, *88*, 3294.
- (25) Frisch, M. J.; Trucks, G. W.; Schlegel, H. B.; Scuseria, G. E.; Robb, M. A.; Cheeseman, J. R.; Montgomery, J. A., Jr.; Vreven, T.; Kudin, K. N.; Burant, J. C.; Millam, J. M.; Iyengar, S. S.; Tomasi, J.; Barone, V.; Mennucci, B.; Cossi, M.; Scalmani, G.; Rega, N.; Petersson, G. A.; Nakatsuji, H.; Hada, M.; Ehara, M.; Toyota, K.; Fukuda, R.; Hasegawa, J.; Ishida, M.; Nakajima, T.; Honda, Y.; Kitao, O.; Nakai, H.; Klene, M.; Li, X.; Knox, J. E.; Hratchian, H. P.; Cross, J. B.; Bakken, V.; Adamo, C.; Jaramillo, J.; Gomperts, R.; Stratmann, R. E.; Yazyev, O.; Austin, A. J.; Cammi, R.; Pomelli, C.; Ochterski, J. W.; Ayala, P. Y.; Morokuma, K.; Voth, G. A.; Salvador, P.; Dannenberg, J. J.; Zakrzewski, V. G.; Dapprich, S.; Daniels, A. D.; Strain, M. C.; Farkas, O.; Malick, D. K.; Rabuck, A. D.; Raghavachari, K.; Foresman, J. B.; Ortiz, J. V.; Cui, Q.; Baboul, A. G.; Clifford, S.; Cioslowski, J.; Stefanov, B. B.; Liu, G.; Liashenko, A.; Piskorz, P.; Komaromi, I.; Martin, R. L.; Fox, D. J.; Keith, T.; Al-Laham, M. A.; Peng, C. Y.; Nanayakkara, A.; Challacombe, M.; Gill, P. M. W.; Johnson, B.; Chen, W.; Wong, M. W.; Gonzalez, C.; Pople, J. A. *Gaussian 03*, Rev. D.01; Gaussian Inc.: Wallingford, CT, 2004.
- (26) Lotz, Ch.; Zellner, R. *Phys. Chem. Chem. Phys.* **2001**, *3*, 2607.
- (27) Spanget-Larsen, J.; Gil, M.; Gorski, A.; Blake, D. M.; Waluk, J.; Radziszewski, J. G. *J. Am. Chem. Soc.* **2001**, *123*, 11253.
- (28) Hamm, P.; Ohline, S. M.; Zinth, W. *J. Chem. Phys.* **1997**, *106*, 519.
- (29) Suzuki, I. *J. Mol. Spectrosc.* **1968**, *25*, 479.
- (30) Gordon, H. R.; McCubbin, T. K. *J. Mol. Spectrosc.* **1966**, *19*, 137.
- (31) Kandratsenka, A.; Schroeder, J.; Schwarzer, D.; Vikhrenko, V. *Phys. Chem. Chem. Phys.* **2007**, *9*, 1688.
- (32) Kandratsenka, A.; Schroeder, J.; Schwarzer, D.; Vikhrenko, V. *Phys. Chem. Chem. Phys.* **2005**, *7*, 1205.